Available online at www.sciencedirect.com
SCIENCE DIRECT®
Journal of Nuclear Materials 345 (2005) 192–205
journal of nuclear materials
www.elsevier.com/locate/jnucmat

On the oxidation state of UO_2 nuclear fuel at a burn-up of around 100 MWd/kgHM

C.T. Walker [a,*], V.V. Rondinella [a], D. Papaioannou [a], S. Van Winckel [a] W. Goll [b], R. Manzel [b]

[a] European Commission, Joint Research Centre, Institute for Transuranium Elements, P.O. Box 2340, D-76125 Karlsruhe, Germany
[b] Framatome ANP GmbH, P.O. Box 3223, D-91050 Erlangen, Germany

Received 6 December 2004; accepted 27 May 2005

Abstract

Results for the radial distribution of the oxygen potential and stoichiometry of a PWR fuel with an average pellet burn-up of 102 MWd/kgHM are presented. The local $\Delta\overline{G}(O_2)$ of the fuel was measured using a miniature solid state galvanic cell, the local O/U ratio was calculated from the lattice parameter measured by micro-X-ray diffraction and the local O/M ratio was derived from the fuel composition determined by ICP-MS. During irradiation the O/U ratio of the fuel decreased from 2.005 to 1.991 ± 0.008. The average fuel O/M ratio was 1.973 compared with the stoichiometric value of 1.949. The amount of free oxygen in the fuel, represented by the difference between these two quantities, increased from the centre to periphery of the pellet. Similarly, the $\Delta\overline{G}(O_2)$ of the fuel increased from -370 kJ mol^{-1} at $r/r_0 = 0.1$ to -293 kJ mol^{-1} at $r/r_0 = 0.975$. Thus, the $\Delta\overline{G}(O_2)$ of the fuel had not been buffered by the oxidation of fission product Mo. About one-quarter of the free oxygen accumulated during the irradiation had been gettered by the Zircaloy cladding.

1. Introduction

The oxidation state is generally acknowledged to be the most important chemical property of UO_2 nuclear fuel during irradiation. This is because the oxygen potential, $\Delta\overline{G}(O_2)$, and the related O/M ratio of the fuel, affect diffusion controlled processes such as grain growth [1], creep [2] and fission gas release [1,3,4], the thermal conductivity of the fuel [5–7] and the chemical state and hence behaviour of the fission products [8]. The $\Delta\overline{G}(O_2)$and O/M ratio of the fuel are not constant during irradiation, but change with burn-up. Davies and Ewart [9] reported on the basis of the calculated composition changes during irradiation that stoichiometric uranium dioxide fuel with an enrichment of 30% ^{235}U oxidises to $UO_{2.004}$ at 10 at.% burn-up. Later, Kleykamp [10,11] performed similar calculations for a stoichiometric UO_2 fuel with an enrichment of 4.3 at.% ^{235}U and proposed that up to a burn-up of 5 at.% an estimate of the average shift in stoichiometry can be obtained from $\Delta(O/M) = 0.0013$ per at.% burn-up. He concluded, however, that in high power (high temperature) fuel rods the excess oxygen is completely gettered by the Zircaloy cladding and consequently the O/M of the fuel remains close to 2.00 during irradiation.

* Corresponding author. Tel.: +49 7247 951 477.
E-mail address: clive.walker@itu.fzk.de (C.T. Walker).

0022-3115/$ - see front matter © 2005 Elsevier B.V. All rights reserved.
doi:10.1016/j.jnucmat.2005.05.010

To the knowledge of the authors only Adamson, Une and Matzke and their coworkers have measured the $\Delta\overline{G}(O_2)$ of irradiated UO_2 nuclear fuel. All of them used a solid electrolyte galvanic cell. Adamson et al. [12] measured the variation in $\Delta\overline{G}(O_2)$ with radial position at 750 °C in two UO_2 fuels with burn-ups of 11.4 and 18.9 MWd/kgHM. The oxygen potential in the fuels varied from -560 kJ mol^{-1} at the centre of the fuel to -450 kJ mol^{-1} at the fuel surface. They estimated that these $\Delta\overline{G}(O_2)$ values corresponded to O/M ratios of about 1.997 and 1.999, respectively. Une et al. [13] carried out $\Delta\overline{G}(O_2)$ measurements at 750 °C on two BWR fuels with burn-ups of 18 and 30 MWd/kgHM. They report that the oxygen potential of the fuels ranged from -480 kJ mol^{-1} in the central region of the pellet to -420 kJ mol^{-1} at the fuel surface and that the higher burn-up increment of 12 MWd/kgHM caused the $\Delta\overline{G}(O_2)$ of the fuel to increase by about 40 kJ mol^{-1}. Matzke [14] measured the $\Delta\overline{G}(O_2)$ of several fuels with burn-ups in the range 30–75 MWd/kgHM with initial enrichments of 1.46 to 8.25 wt% ^{235}U. At 750 °C the $\Delta\overline{G}(O_2)$ of all but one of the fuels was close to -400 kJ mol^{-1} which corresponds to the $\Delta\overline{G}(O_2)$ of the reaction $Mo + O_2 \rightarrow MoO_2$. After taking into consideration the dissolved rare-earth fission products and the Pu formed during irradiation, he concluded that some of the fuels investigated were slightly hypostoichiometric and that the highest possibly degree of oxidation corresponded to $UO_{2.001}$. Earlier, Matzke [15] had published $\Delta\overline{G}(O_2)$ results for the rim region of the fuel with the highest burn-up of 75 MWd/kgHM. The samples investigated were taken from within 200 μm of the pellet surface where a steep burn-up gradient existed. EPMA results for the Nd concentration in this region of the fuel [16] indicate that the average burn-up of the samples was probably about 150 MWd/kgU rather than in excess 200 MWd/kgHM as stated by Matzke [15]. At 750 °C, the $\Delta\overline{G}(O_2)$ of the rim samples lay in the range -460 to -420 kJ mol^{-1}, to which Matzke attributed a local O/M between 1.996 and 2.000. This implies that despite the fact that almost all of the accumulated burn-up in the rim region was the result of Pu fission (the fuel enrichment was 1.46 wt% ^{235}U) the fuel had not oxidised.

The relation between the $\Delta\overline{G}(O_2)$ and O/M ratio of unirradiated uranium dioxide is well known (see e.g., Fig. 5, Ref. [15]). In contrast, the translation of the oxygen potential of irradiated uranium dioxide nuclear fuel to O/M is associated with large uncertainties. This is because allowances have to be made for dissolved fission productions and plutonium in the uranium dioxide lattice, which involves many assumptions. Marken and Bones [17] were probably the first to produce reliable measurements of the $\Delta\overline{G}(O_2)$ of uranium dioxide as a function of O/M. Since they claimed that hypostoichiometric uranium dioxide exists only at temperatures above 1300 °C, they restricted their work to the measurement of the $\Delta\overline{G}(O_2)$ of stoichiometric and hyperstoichiometric uranium dioxide at 850 °C. They found that the $\Delta\overline{G}(O_2)$ changed dramatically at stoichiometric composition. Thus, the $\Delta\overline{G}(O_2)$ of hyperstoichiometric uranium dioxide was around -230 kJ mol^{-1}, whereas the $\Delta\overline{G}(O_2)$ of stoichiometric uranium dioxide was about -420 kJ mol^{-1}. These results have been confirmed by later workers (see Fig. 5, Ref. [15]). The O/M of irradiated nuclear fuel has been estimated from an oxygen balance, which presumes that the chemical state of the fission products is known [8,9], or inferred from $\Delta\overline{G}(O_2)$ measurements on unirradiated uranium dioxide doped with fission product elements and of known O/M ratio [15,18–21]. The O/M ratio of irradiated nuclear fuel can in theory also be obtained from lattice parameter measurements. The interpretation of the results, however, is not straightforward because the lattice parameter of irradiated UO_2 is not only affected by the local O/U ratio, but also by the local concentrations of fission products and plutonium dissolved in the fuel lattice and the level of radiation damage [22–24].

The present paper reports the results of oxygen potential measurements made on a commercial PWR fuel with an average burn-up of 102 MWd/kgHM using a miniature galvanic cell. The irradiated fuel has been characterised in detail using a wide range of post-irradiation examination techniques. The radial distributions of fission product neodymium and plutonium were measured by electron probe microanalysis (EPMA). The local neodymium concentration is used as an indicator of the local burn-up and also as a pointer to the behaviour of the other rare-earth fission products. Moreover, the variation of the lattice parameter across the fuel radius has been measured by micro-X-ray diffraction and the concentration of fission products dissolved in the fuel lattice has been determined by inductively coupled plasma mass spectrometry (ICP-MS). In addition, the extent of formation of the high burn-up structure in the fuel has been established using optical microscopy and scanning microscopy. The lattice parameter results and the fission product inventory data are used to estimate the local O/U and O/M ratio of the fuel, respectively, and its variation with radial position. Thus, the paper provides a comprehensive picture of the oxidation state of LWR fuel at ultra high burn-up.

2. Fuel characteristics and irradiation history

The fuel pellet and rod design characteristics are given in Table 1. It is seen that the fuel had a standard enrichment of 3.5% and was slightly hyperstoichiometric. The fuel rod cladding was a highly corrosion resistant zirconium alloy.

The high burn-up rod was of standard Siemens PWR design with plenum space above and below the fuel

Table 1
Fuel pellet and rod design characteristics

Pellet diameter (mm)	9.3
Initial enrichment (wt% ^{235}U)	3.5
Fuel density (%TD)	95
2D grain size[a] (μm)	9–12
O/M	2.005
Diametrical gap (μm)	160–190
He fill gas pressure (bar)	22.5
Cladding material	Zr-based alloy

[a] Linear intercept.

Table 2
Power history and burn-up evolution in the high burn-up fuel rod

Reactor cycle	Max. Av. linear power (kW m^{-1})	Cumulative Av. burn-up (MWd/kgHM)
1	34	19
2	29	37
3	23	48
4	20	59
5	18	67
6	17	72
7	16	82
8	14	90
9	14	98

stack. It was irradiated in a commercial PWR reactor in a Siemens built 15×15 fuel assembly. The irradiation spanned nine reactor cycles and lasted about 3000 effective full power days (EFPD). At the end of the fourth irradiation cycle, when the original fuel assembly had reached a burn-up in the region of 60 MWd/kgHM, the rod was transferred to a carrier assembly containing partially burnt fuel. The rod was then subsequently introduced into a new carrier assembly at the start of each reactor cycle.

From Table 2 it is seen that during the first four reactor cycles the average power rating fell from 34 to 20 kW m^{-1}. During irradiation in the carrier assemblies the power rating decreased gradually from 18 kW m^{-1} in the fifth irradiation cycle to 14 kW m^{-1} in the ninth and final cycle. The rod average burn-up at the end-of-life was 97.8 MWd/kgHM.

3. Fuel sample on which the oxygen potential measurements were made

The high burn-up fuel sample on which the oxygen potential measurements were made was a 1 mm thick disc cut from the upper end of the fuel stack within 15 mm of the location of the samples on which optical microscopy, EPMA and SEM were performed. The average burn-up of the disc, therefore, was similar to that of these samples, which was taken to be 102 MWd/kgHM. The burn-up was determined by dissolving adjacent fuel pellets in 6 M nitric acid and then establishing the ratio of the ^{148}Nd concentration and the U and Pu concentrations in the solution using inductively coupled plasma mass spectrometry (ICP-MS). The fission yield of ^{148}Nd was taken to be 1.75%. This represents the average through life yield resulting from thermal fission of ^{239}Pu, ^{241}Pu and ^{235}U and the fast fission of ^{238}U. For conversion of the burn-up from at.% to MWd/kgHM it was assumed that 1 at.% was equal to 9.65 MWd/kgHM. This corresponds to a fission energy of about 207 MeV.

An important variable that influences the local oxygen potential of nuclear fuel during irradiation is the radial temperature profile since this dictates the oxygen distribution [25]. The high burn-up rod was irradiated at low temperature. During the first two irradiation cycles the fuel centre temperature was in the range 1200–1400 °C, thereafter the centre temperature was around 900 °C.

4. Post-irradiation examination results relevant to this study

4.1. EPMA results for the radial distribution of neodymium

Neodymium is immobile in UO_2 nuclear fuel and therefore can be used as an indicator of the radial burn-up distribution and the local concentration of fission products in the fuel lattice. The radial distribution of Nd in the fuel was measured by EPMA using the procedure described in Ref. [26]. The resulting concentration profile is shown in Fig. 1. It can be seen that in

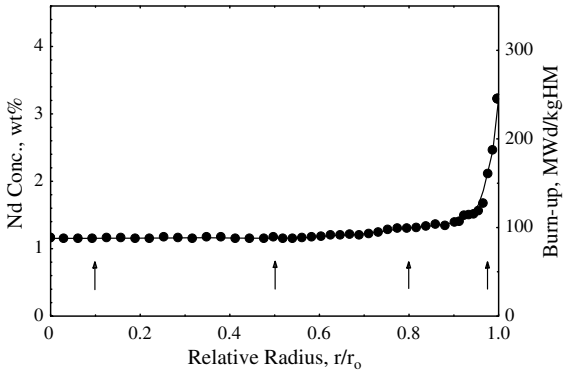

Fig. 1. EPMA results for radial distribution of Nd in the high burn-up fuel. The burn-up values shown on the right ordinate were calculated assuming that the integral average Nd concentration of 1.34 wt% corresponds to the pellet burn-up of 102 MWd/kgHM. The arrows mark the four radial locations where $\Delta\overline{G}(O_2)$ measurements were made.

Table 3
EPMA results for the local concentrations of neodymium, caesium, xenon and plutonium at the radial locations where the oxygen potential was measured and the local burn-up at the same locations determined from the measured neodymium concentration

Radial position (r/r_0)	Local burn-up (MWd/kgHM)	Concentration (wt%)			
		Neodymium	Caesium	Xenon	Plutonium
0.1	88.3	1.16	0.10	0.17	1.40
0.5	88.3	1.16	0.32	0.18	1.41
0.8	97.8	1.31	0.62	0.21	1.54
0.975	161.4	2.12	0.96	0.30	2.47

the interior of the fuel the Nd distribution is flat, whereas at the pellet surface the Nd concentration increases steeply due to the fission of Pu created by neutron capture [27]. Arrows mark the four radial locations where $\Delta\overline{G}(O_2)$ measurements were made. The local concentration of Nd at these locations and the equivalent local burn-up derived assuming that the integral average concentration of Nd, 1.34 wt%, corresponds to a pellet burn-up of 102 MWd/kgHM is given in Table 3. The burn-up information obtained from the radial Nd profile was used to correct the lattice parameter measurements (see Section 4.4) and together with the ICP-MS results formed the basis for the oxygen balance calculations described in Section 5.4.

4.2. EPMA results for the radial distributions of xenon and caesium

The EPMA procedures used for the analysis of Xe and Cs are reported in Refs. [26,28]. The measured radial concentration profiles are shown in Fig. 2. It can be seen from the figure that over the whole pellet cross-section only a small fraction (0.15–0.3 wt%) of the created Xe concentration (pellet average 1.4 wt%) is retained in the fuel grains. The behaviour of Cs was noticeably different to that of Xe. As seen from Fig. 2, Cs is completely retained in the outer region of the fuel. In the region between $r/r_0 = 0.6$ and the fuel centre Cs has been released and its concentration in the fuel grains decreases to about 0.1 wt% at the centre of the fuel. Again, the local concentrations of Xe and Cs at the four radial locations where the $\Delta\overline{G}(O_2)$ measurements were made are listed in Table 3.

4.3. EPMA results for the radial distribution of plutonium

When analysing Pu in UO_2 by EPMA a correction is needed for X-ray line interference between U and Pu. A description of the procedure used for the EPMA of Pu can be found in Ref. [28]. The creation of plutonium during irradiation of UO_2 nuclear fuel is the result of the capture of epithermal neutrons in the resonances of ^{238}U. The measured radial concentration profile for Pu

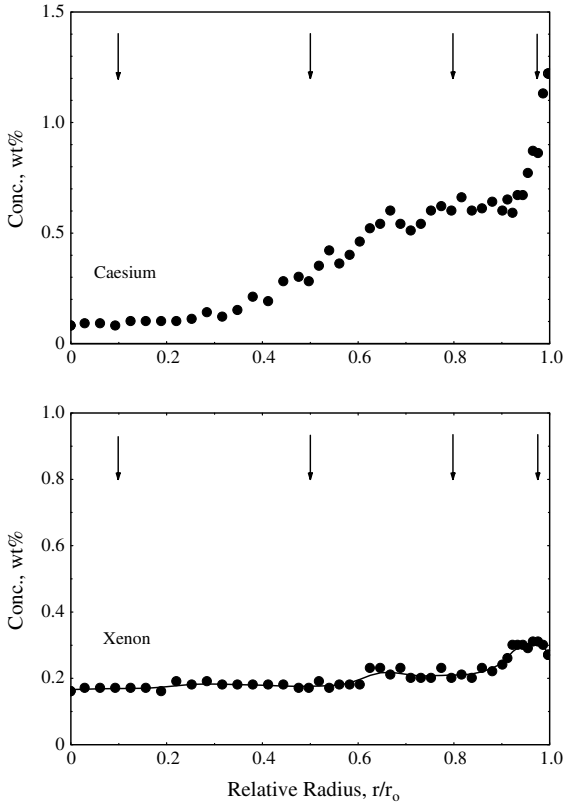

Fig. 2. EPMA results for the radial distribution of Cs and Xe in the high burn-up fuel. The arrows mark the four radial locations where $\Delta\overline{G}(O_2)$ measurements were made.

is shown in Fig. 3. Like the radial profile for Nd, that for Pu is flat in the interior of the fuel and increases steeply at the fuel rim. Clearly, the Pu profile represents the concentration of Pu remaining at the end of the irradiation. Since the fuel burn-up was 102 MWd/kgHM and the initial enrichment was 3.5 wt% ^{235}U, the burn-up accumulated after the third irradiation cycle resulted mainly from the fission of Pu. Thus, substantially more Pu was created (about 7 wt%) during the irradiation than remains at the end of the irradiation (1.6 wt%). Table 3 lists the Pu concentrations measured at the four radial locations where $\Delta\overline{G}(O_2)$ measurements were performed.

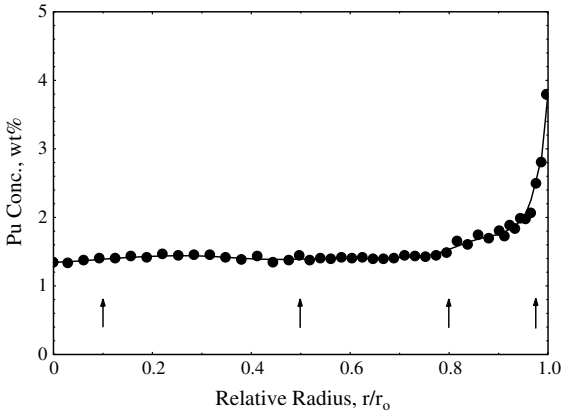

Fig. 3. EPMA results for the radial distribution of Pu in the high burn-up fuel. The arrows mark the four radial locations where $\Delta\overline{G}(O_2)$ measurements were made.

4.4. Lattice parameter measurements by micro-X-ray diffraction

As pointed out in Section 1, the lattice parameter of irradiated UO_2 nuclear fuel is influenced by the oxidation state of the fuel, by the concentrations of fission products and Pu dissolved in the fuel lattice and by the level of radiation damage. Spino and Papaioannou [29] have measured the variation in the lattice parameter across the fuel radius using micro-XRD. A description of the experimental set-up and measurement procedure is given in Ref. [24]. The lattice parameter results are shown in Fig. 4. It can be seen that the lattice parameter profile exhibits two distinct humps which are attributed to lattice strain caused by radiation damage. In the outermost hump, the lattice parameter peaks at 547.6 pm after which it decreases to 547.0 pm at the fuel surface.

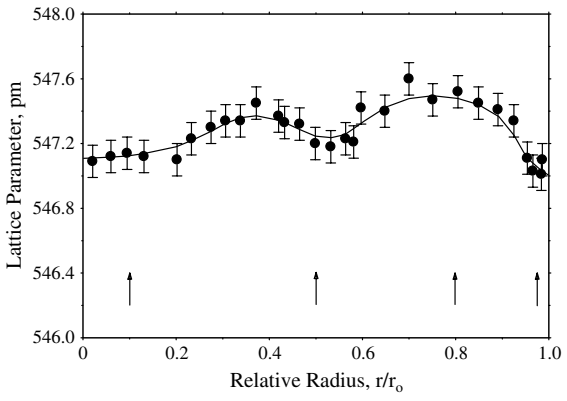

Fig. 4. Radial variation in the lattice parameter of the high burn-up fuel as measured by micro-X-ray diffraction (after Spino, Ref. [29]). The arrows mark the four radial locations where $\Delta\overline{G}(O_2)$ measurements were made.

The distance over which the lattice parameter decreases in the outer region of the fuel coincides with the penetration depth of the high burn-up structure in this region. At the centre of the fuel out to $r/r_0 = 0.2$ the average value of the lattice parameter was 547.1 pm. It is assumed that throughout the irradiation the fuel temperature in this region was high enough to inhibit radiation damage and consequently lattice strain.

The uncertainty on the local lattice parameter is less than ±0.1 pm [24] which corresponds to about 0.02% relative.

5. Methods

5.1. Oxygen potential measurements

A miniature solid state galvanic cell contained in an inert atmosphere glove box was used for the measurement of the oxygen potential. Matzke [14,15] provides a diagram and description of the cell in its current form. Briefly, it consists of a reference electrode, (Fe/FeO)/Pt, the working electrode, Pt/nuclear fuel, and a ThO_2–Y_2O_3 electrolyte in which the conductivity is due exclusively to the migration of oxygen. The electrolyte is a yttria-doped thoria crucible with a Pt-lid which is spring-loaded to ensure good contact with the sample and prevent the developing oxygen pressure from being pumped away during evacuation. Electrical contact to the lid and the reference electrode is made by the Pt wires of the Pt/Pt–10%Rh thermocouple. The cell is suspended in an alumina tube connected to the vacuum system.

When thermal equilibrium is reached, the reversible emf, E, between the working and reference electrodes is related to the oxygen potentials by the Nernst equation:

$$E\ [\mathrm{mV}] = \frac{RT}{4F}\mathrm{Ln}\frac{\mu_{O_2}^{\mathrm{fuel}}}{\mu_{O_2}^{\mathrm{ref.}}}\ [\mathrm{kJ\ mol^{-1}}], \tag{1}$$

where R is the gas constant, T is the absolute temperature, F is the Faraday constant and μ_{O_2} is the oxygen activity. Under the conditions of the galvanic cell, μ_{O_2} can be approximated by the oxygen partial pressure, p_{O_2}. Since the oxygen potential of the reference electrode is known, the oxygen potential of the sample can be determined.

Oxygen potential measurements were carried out on four pieces of fuel weighing a few milligrams chipped from a large, roughly triangular (slice-of-pie) fragment of the disk sample (see Section 3). The base of the triangular fragment corresponded to the periphery of the pellet, hence to the highest burn-up region. The centre of the pellet, included in the triangular piece, corresponded to a region near the apex of the triangle. The radial location from which the four pieces of fuel were taken approximated to $r/r_0 = 0.1$, representing the centre of

the pellet, $r/r_0 = 0.5$, $r/r_0 = 0.8$ and $r/r_0 = 0.975$ representing the pellet rim. $\Delta\overline{G}(O_2)$ measurements were performed in the temperature range 625–1125 °C. Before each measurement campaign, unirradiated UO_{2+x} of known O/U ratio (typically stoichiometric $UO_{2.00}$) was analysed as a reference to ensure that the galvanic cell was functioning correctly and to minimise errors. On each sample of irradiated fuel several runs consisting of repeated temperature cycles were made in order to obtain stable and reproducible readings of the emf. Successful measurements were performed on all samples, with the exception of the one from the pellet centre. For this sample, stable readings of the emf potential were not obtained after several runs.

5.2. Inductively coupled plasma mass spectrometry

ICP-MS was carried out on 2 ml aliquots of diluted fuel solution using an ELEMENT 2 instrument (Thermo Electron GmbH, Germany) which has been modified to handle radioactive samples in a glove box. The fuel solution was prepared in a hot cell by adding a sample of fuel weighing 7.070 g to 50 ml of 4 M HNO_3. Of this weight of fuel, 6.874 g dissolved completely, 0.166 g remained as residue and 0.029 g, representing 0.43% of the sample weight, were lost during centrifuging and filtration. The resulting fuel solution was diluted in two steps to a dilution factor of 4.6×10^4 and then in a third step to a dilution factor 1.1×10^6. The solution with the former dilution was used principally for the analysis of the fission products and the higher actinides, and the solution with the latter dilution was used mainly for the analysis of ^{238}U and ^{239}Pu. Dilution of the fuel solution was necessary to reduce its radioactivity to a level that could be safely handled in a glove box and to ensure that the isotope intensities were in the linear dynamic range of the analyser. To correct for the instrumental drift during the measurement sequence, In, Ho and Th were added as internal standards at a concentration level of nanograms per gram in the two final dilutions. Blank solutions were prepared following the same scheme of dilutions and addition of internal standards. Calibration curves were produced using a series of dilutions of certified multi-element standard solutions (multi-element calibration standards 1, 2a, 3 and 4, Agilent Technologies, Germany) in the concentration range of the major elements in the fuel solutions. The same internal standards were also added to these standard solutions.

All measured concentrations were corrected for instrumental drift by means of the internal standards, and the intensities of the blank solutions were subtracted. The fission product concentrations were determined using the calibration curves for the stable natural isotopes in the dilutions of the standard solutions, whereas the concentrations of all the actinides were determined from a single calibration curve for ^{238}U (without mass bias correction). For all isotopes at a concentration level within the calibration range, the results from the two dilutions agreed within 5%. The concentrations of the elements were calculated from the isotopic data. Isobaric interferences were separated using the isotope ratios calculated with the ORIGEN code [30] as a reference. For the interferences $^{134}Cs/^{134}Ba$, $^{137}Cs/^{137}Ba$, $^{154}Gd/^{154}Eu$ and $^{155}Gd/^{155}Eu$, the respective contributions of the isotopes could not be determined with certainty, and hence the 134 and 137 mass peaks were assumed to consist entirely of Cs and the 154 and 155 mass peaks entirely of Gd. A realistic value for the uncertainty on the reported element concentrations is judged to be 10% (1s).

The fuel solution was prepared in July 1998 when it was used for chemical burn-up analysis, which involved the analysis of the Nd, U and Pu isotopic composition of the fuel. The full fission product and actinide analysis of the fuel reported in this paper was carried out in January 2004. Evaporation of the solution and corresponding concentration of the isotopes in the intervening period was corrected for by applying to all the measured isotope concentrations a correction factor of 0.82 obtained from the observed increase in the concentrations of Nd, Pu and U.

5.3. Derivation of the O/U ratio from the lattice parameter

The lattice parameter of irradiated UO_2 is affected by the concentrations of fission products and plutonium incorporated in the lattice, by lattice strain from radiation damage in-pile, and by alpha-damage during storage after discharge from the reactor. Thus, to determine the lattice parameter corresponding to the fuel O/U, the measured lattice parameter must be corrected for the effects of dissolved fission products, plutonium, radiation damage and alpha-damage during storage.

The correction for the concentrations of Y, Sr, the rare-earths and Zr dissolved in the UO_2 lattice was made using the tabulated data for the lattice parameter change caused by single fission products at a concentration level of 1 at.% given by Benedict et al. [23]. The local concentration of fission products at the radial positions where the lattice parameter was measured was calculated by multiplying the ICP-MS results for the average concentration of the fission products in the fuel by the local burn-up represented as a fraction of the average burn-up. The local burn-up data was derived from the radial Nd profile measured by EPMA (Fig. 1). At the pellet burn-up of 102 MWd/kgHM, dissolved fission products resulted in a decrease in the lattice parameter of 1.181 pm. The value assumes that all the Zr present was dissolved in the UO_2 lattice.

The incorporation of plutonium also lowers the lattice parameter of UO_2. The effect of a known concentration

of PuO_2 on the lattice parameter of UO_2 was calculated using Vegard's Law [31] taking the lattice parameters of $PuO_{2.00}$ and $UO_{2.00}$ to be 539.20 and 547.02 pm, respectively. The local mole fraction of PuO_2 at the radial positions where the lattice parameter was measured was obtained by multiplying the average concentration of Pu in the fuel measured by ICP-MS, by the local fraction of the average concentration of Pu in the fuel cross-section derived from the radial Pu profile measured by EPMA (Fig. 3). The fuel contained 1.37 mol% PuO_2, which resulted in a relatively small decrease in lattice parameter of 0.107 pm.

Alpha radiation damage during storage of spent fuel causes an increase in the lattice parameter. The change in the lattice parameter during storage was obtained from the number of displacements per atom (dpa). This in turn was calculated from the specific activity of the fuel and the time elapse between discharge of the fuel from the reactor and the measurement of the lattice parameter. The relation between the lattice parameter and dpa was provided by experimental data from a long term study at ITU of the evolution of the lattice parameter of UO_2 doped with 10 wt% ^{238}Pu [32].

From the isotopic compositions of the actinide elements measured by ICP-MS (see Table 4) the specific activity of the fuel was calculated to be 4.5×10^9 Bq g^{-1}. More than 95% of this activity is generated by ^{244}Cm. Assuming that an alpha decay event causes 1750 atomic displacements, then during the 37 months that had elapsed between the discharge of the fuel from the reactor and the measurement of the lattice parameter, alpha decay will have resulted in 0.086 dpa. From the investigation of ^{238}Pu doped UO_2 at ITU [33] this degree of damage results in an increase in the lattice parameter of about 0.21%. At those radial positions where lattice parameter measurements were made the increase in the lattice parameter due to alpha radiation damage during storage was calculated from the local Pu concentration measured by EPMA (Fig. 3), which was used as an indicator of the local specific activity and hence local damage in terms of dpa.

After the lattice parameter measurements had been corrected for the local concentrations of dissolved fission products and plutonium, and for alpha-damage, they were corrected for the lattice strain resulting from in-pile radiation damage. This involved removing the two humps in the lattice parameter profile between $r/r_0 = 0.25$ and 0.49 and $r/r_0 = 0.59$ and 0.94, which are attributed to radiation damage (Fig. 4). It is assumed that between the centre of the fuel and $r/r_0 = 0.25$ the temperature during irradiation was sufficiently high to anneal the radiation damage, and that in the radial interval between the two humps where recrystallisation had occurred [29] radiation damage was also absent. This is consistent with the lower lattice parameters measured in these regions.

Table 4
ICP-MS results for the average composition of the fuel

Element	Concentration (wt%)	Remarks
Rb	0.073	
Sr	0.175	
Y	0.092	
Zr	0.913	
Mo	0.346	Major residue component
Tc	0.032	Idem
Ru	0.112	Idem
Rh	0.014	Idem
Pd	0.235	Idem
Cd	0.065	Omitting Cd-113 (minor isotope)
Sn	0.010	Omitting Sn-119 (owing to U^{2+} interference)
Sb	0.003	
Te	0.136	
Cs	0.881	Contributions from Ba-134 and Ba-137
Ba	0.435	Ba-136 and Ba-138 only
La	0.345	
Ce	0.687	
Pr	0.303	
Nd	1.159	
Sm	0.026	
Eu	0.026	Eu-153 only
Gd	0.165	Possible contributions from Eu-154 and Eu-155
Tb	0.004	
Dy	0.017	
Np	0.087	
U	78.162	
Pu	1.229	Residue component also
Am	0.180	
Cm	0.137	

The O/U ratio was derived from the corrected lattice parameter using the data of Grønvold [34] for hyperstoichiometric UO_2 reported in the Gmelin Handbook [35] after extrapolating it to O/U = 1.96. The change in lattice parameter, a, as a function of O/U ratio is described by the relationship

$$a = -0.1367(O/U) + 574.420.$$

The uncertainty on the calculated O/U ratio resulting from the error on the measured lattice parameter is ±0.008.

5.4. Calculation of the O/M from the fuel composition

The calculation of the fuel O/M from its composition involved three steps. First, the pellet composition at the end-of-life was determined. Second, the local composition of the fuel at the four radial positions where the

oxygen potential was measured was calculated. Third, the oxygen in the fuel was distributed between the actinide elements and fission products in solid solution and the fission products that had formed second phases. The fuel composition was determined from the ICP-MS results for the dissolved fraction of the fuel after correcting the measured concentrations of Pu and the period five metals (Mo, Tc, Ru, Rh and Pd) for the amounts of these elements in the residue. The concentration of oxygen in the fuel was derived from the as-fabricated O/U ratio of the fuel of 2.005. The local concentrations of the fission products and actinides, except Pu, Cs, Xe and Kr, were obtained by normalising the pellet composition to the local burn-up derived from the EPMA Nd radial concentration profile (Fig. 1).

The local concentration of Pu was obtained from the EPMA radial concentration profile (Fig. 3). Likewise, the local concentrations of Xe and Cs in the fuel grains at the end-of-life were extracted from the EPMA radial concentration profiles for these fission products shown in Fig. 2. The local concentration of Kr was obtained from the Xe concentration and the measured Xe/Kr ratio of the puncture gas, which was 10.8. It is to be noted that in the central region of the fuel, a large fraction of Cs and the fission gases Xe and Kr had been released to the rod free volume, whilst in the outer region of the fuel Xe and Kr had accumulated in the pores of the high burn-up structure.

For the calculation of the local O/M ratio, the oxygen in the fuel was distributed between the actinide elements, the fission products in solid solution and the fission products that had formed oxide second phases. Uncertainties about the chemical state of the fission products Zr, Mo and Cs are the main source of error in the reported O/M values. To be consistent with its contribution to the change in the lattice parameter caused by dissolved fission products [23], all the Zr present was considered to be in solid solution. All the Mo detected by ICP-MS was considered to have been present in the fuel as a MoO_2 second phase. Caesium was assumed to be in the form of Cs_2O as a separate phase. According to Kleykamp [36] the maximum solubility of Cs in hypostoichiometric UO_2 is around 0.05 at.%. Consideration of the relative sizes of the Cs^+ and U^{4+} ions alone indicates that the solubility of Cs in UO_2 is limited [37].

5.5. Calculation of the stoichiometric O/M ratio

The stoichiometric O/M ratio is the average O/M ratio which results when all the fission products and actinides in the fuel combine with oxygen to form stoichiometric oxides. For the calculation of the stoichiometric O/M ratio it was assumed that all the fission products considered formed their stoichiometric oxides. For the attribution of oxygen, a valence of +4 was assumed for all the actinide and a valence of +3 for all the rare-earth fission products except Ce, which was considered to take a valence of +4 [38].

6. Results

6.1. Radial variation in the oxygen potential

Fig. 5 shows the $\Delta\overline{G}(O_2)$ values measured during the last run on each of the fuel samples. It can be seen that the $\Delta\overline{G}(O_2)$ of all the samples lies above the range of values measured on unirradiated stoichiometric UO_2. Moreover, the $\Delta\overline{G}(O_2)$ of the high burn-up fuel increased noticeably with distance from the pellet centre. Further, for all the fuel samples, except that from the pellet centre, the $\Delta\overline{G}(O_2)$ increased with the measurement temperature. For the fuel samples taken at $r/r_0 = 0.50$, 0.80 and 0.975 the slopes of the oxygen potential curves are similar and the oxygen potential increases by 40 to 55 kJ mol^{-1} over the temperature range in which the measurements were carried out. In contrast, the oxygen potential of the sample from the pellet centre ($r/r_0 = 0.1$) changes little with increase in the measurement temperature. As already mentioned in Section 5.1, for this sample, stable emf potential readings were

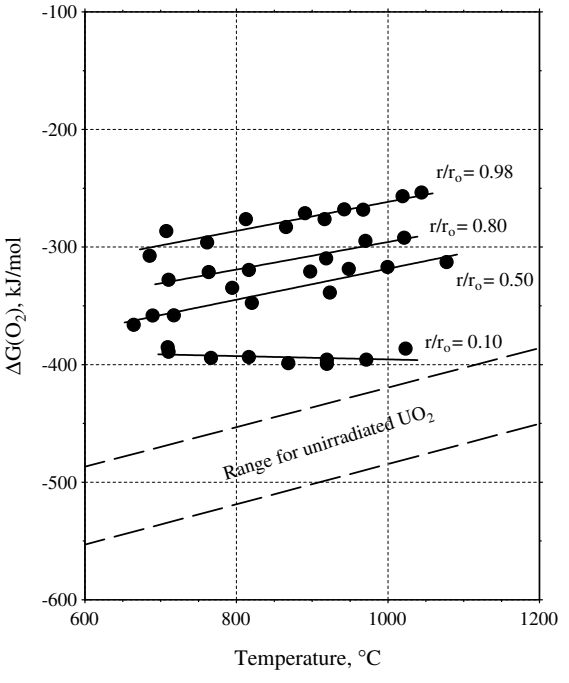

Fig. 5. The $\Delta\overline{G}(O_2)$ at four different radial positions in the high burn-up fuel as a function of temperature. The range of $\Delta\overline{G}(O_2)$ values measured on unirradiated UO_2 is included for the purposes of comparison.

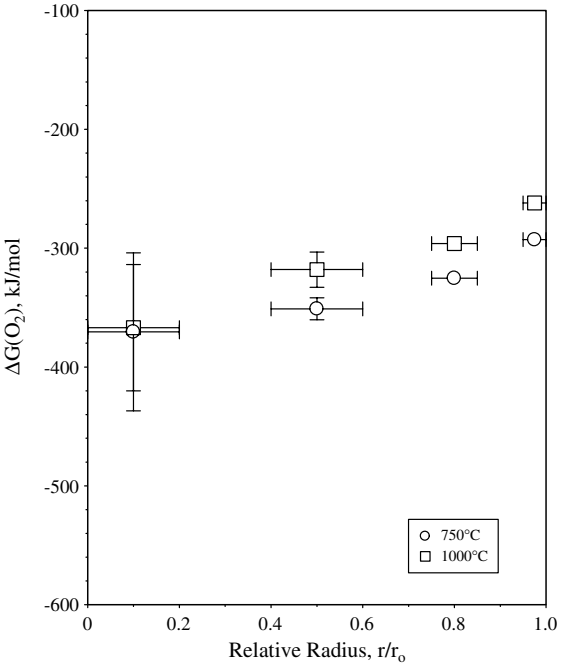

Fig. 6. Variation in the $\Delta\overline{G}(O_2)$ of the high burn-up fuel as a function of the radial position at 750 and 1000 °C.

not obtained, although seven measurement runs were performed. Consequently, a large uncertainty is associated with the oxygen potential values reported for this sample.

In Fig. 6 the $\Delta\overline{G}(O_2)$ values measured at 750 and 1000 °C are shown as a function of the radial position in the high burn-up fuel. These temperatures correspond to the upper and lower limits of the temperature range in which the oxygen potential of the samples was measured. It is seen from the figure that the $\Delta\overline{G}(O_2)$ of the fuel increases (becomes less negative) from the centre to the surface of the fuel. The increase is of the order of 80 kJ mol^{-1} at 750 °C and 105 kJ mol^{-1} at 1000 °C. It is to be noted that the increase in $\Delta\overline{G}(O_2)$ becomes steeper at the fuel rim similarly to the local burn-up profile. The large error bars on the $\Delta\overline{G}(O_2)$ data points at $r/r_0 = 0.1$ reflect the fact that reproducible values of the emf potential were not obtained on the fuel sample.

6.2. Radial variation in the O/U ratio as derived from the lattice parameter

In Fig. 7(a) the lattice parameter corrected for fission products and Pu incorporated in the UO_2 lattice and for lattice strain due to fission and alpha-decay damage is plotted as function of radial position. The figure shows that after varying between 547.12 and 547.26 pm in the central region of the fuel, the lattice parameter decreases

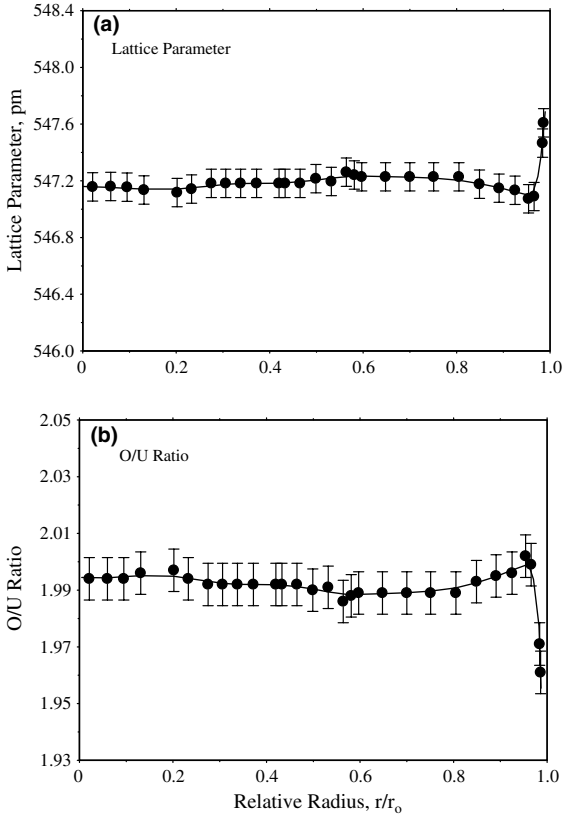

Fig. 7. (a) Radial variation in the lattice parameter after correction for the concentrations of fission products and Pu incorporated in the UO_2 lattice, lattice strain from in-pile radiation damage and alpha-damage during storage after discharge from the reactor; (b) radial variation in the O/U ratio derived from the corrected lattice parameter.

slightly to 547.07 pm in the outer region of the fuel before increasing steeply to 547.61 pm at the pellet rim. The O/U ratios derived from the lattice parameter values plotted in Fig. 7(a) are shown in Fig. 7(b). It can be seen that in the body of the fuel the O/U ratio decreases slightly from 1.994 ± 0.008 at the fuel centre to 1.989 ± 0.008 at $r/r_0 = 0.70$. It then increases to 2.002 ± 0.008 at $r/r_0 = 0.95$ before dropping sharply to 1.961 ± 0.008 at $r/r_0 = 0.99$. Thus, the lattice parameter data indicates that, over most of its radius the high burn-up fuel matrix was slightly hypostoichiometric. The rim region of the fuel constitutes the exception; within 100 μm of the pellet surface the degree of hypostoichiometry increased dramatically.

6.3. Radial variation in the O/M ratio as derived from the fuel composition

Table 4 gives the ICP-MS results for the mass concentrations of the fission products and actinides in

Table 5
The oxygen balance in at.% and resulting O/M ratios at the radial positions where the oxygen potential was measured

Elements in solid solution		Radial position, r/r_0, and local burn-up			
		0.10 (88 MWd/kgHM)	0.50 (88 MWd/kgHM)	0.80 (100 MWd/kgHM)	0.975 (162 MWd/kgHM)
Heavy metals	U	29.292	29.247	28.654	25.932
	Np	0.028	0.028	0.031	0.050
	Pu	0.510	0.509	0.577	0.919
	Am	0.056	0.056	0.063	0.101
	Cm	0.042	0.042	0.048	0.076
Fission products	Sr	0.146	0.146	0.165	0.265
	Y	0.078	0.078	0.089	0.141
	Zr	0.740	0.740	0.837	1.333
	La	0.187	0.187	0.212	0.337
	Ce	0.367	0.367	0.416	0.662
	Pr	0.162	0.162	0.183	0.292
	Nd	0.611	0.610	0.691	1.101
	Sm	0.103	0.103	0.117	0.186
	Eu	0.013	0.013	0.015	0.023
	Gd	0.080	0.080	0.091	0.144
	Tb	0.002	0.002	0.002	0.003
	Dy	0.008	0.008	0.009	0.015
Concentration in solid solution (1)		32.425	32.387	32.200	31.578

Oxide second phases	Metal	Oxygen	Metal	Oxygen	Metal	Oxygen	Metal	Oxygen
BaO	0.238	0.238	0.237	0.237	0.269	0.269	0.428	0.428
MoO_2	0.264	0.528	0.263	0.526	0.298	0.596	0.475	0.950
Cs_2O	0.059	0.030	0.208	0.104	0.401	0.201	0.596	0.298
Concentration of oxygen in second phases (2)	0.796		0.867		1.066		1.676	
Oxygen concentration in the fuel (3)	65.052		64.951		64.602		63.397	
Fuel O/M ratio {(3) − (2)}/(1)	1.982		1.979		1.973		1.955	

the fuel. The concentrations reported for the period five elements, Mo, Tc, Ru, Rh and Pd, and for Pu are low because they are also constituents of the residue remaining after dissolution of the fuel. The fission products Nb and Pm, which as oxides are miscible with UO_2, were not detected. Oxygen and the fission gases Xe and Kr can not be measured by solution ICP-MS.

Table 5 lists the concentrations in at.% of the elements in solid solution and in oxide second phases together with the theoretical oxygen balance. It can be seen from the table that the theoretical oxygen balance based on the local composition of the fuel indicates that the fuel O/M decreased from 1.982 in the central region of the fuel to 1.955 close to the pellet surface.

The amount of oxygen that must react with the fission products and actinides in the fuel lattice to produce stoichiometric oxides and the resulting average O/M ratio from these data are given in Table 6. It can be seen that the stoichiometric O/M ratio decreases from 1.967 at $r/r_0 = 0.1$ to 1.948 at $r/r_0 = 0.8$ before decreasing to 1.918 at $r/r_0 = 0.975$.

7. Discussion

The finding that the $\Delta\overline{G}(O_2)$ of the high burn-up fuel investigated in this work lies above the range of values measured on unirradiated stoichiometric UO_2 is consistent with the knowledge that dissolved rare-earth fission products increase the $\Delta\overline{G}(O_2)$ of UO_2 [19,20]. Not only is the $\Delta\overline{G}(O_2)$ of the high burn-up fuel higher than that of unirradiated stoichiometric UO_2 it is also markedly higher than the values reported for high burn-up fuel by Matzke [14]. He found that the $\Delta\overline{G}(O_2)$ of UO_2 fuel with a pellet burn-up of 75 MWd/kgU varied from −470 to −380 kJ mol^{-1} at 750 °C. In the present work $\Delta\overline{G}(O_2)$ values in the range −390 to −290 kJ mol^{-1} were measured at this temperature (see Fig. 1). The difference in the $\Delta\overline{G}(O_2)$ values measured is attributed to the difference in burn-up of the fuels investigated. As mentioned above, the fuel studied by Matzke had an average burn-up of 75 MWd/kgU, whereas the average burn-up of the fuel investigated in this work was 102 MWd/kgU. Thus, the fission product inventory of the high burn-up fuel in this work was substantially higher.

Table 6
The concentration of oxygen in at.% bound to the actinides and fission products and the resulting average O/M ratio

Elements in solid solution		Valence	Radial position, r/r_0, and local burn-up							
			0.10 (88 MWd/kgHM)		0.50 (88 MWd/kgHM)		0.80 (100 MWd/kgHM)		0.975 (162 MWd/kgHM)	
			Metal	Oxygen	Metal	Oxygen	Metal	Oxygen	Metal	Oxygen
Heavy metals	U	4	29.292	58.584	29.247	58.494	28.654	57.308	25.932	51.864
	Np	4	0.028	0.056	0.028	0.056	0.031	0.062	0.050	0.100
	Pu	4	0.510	1.020	0.509	1.018	0.577	1.154	0.919	1.838
	Am	4	0.056	0.112	0.056	0.112	0.063	0.126	0.101	0.202
	Cm	4	0.042	0.084	0.042	0.084	0.048	0.096	0.076	0.152
Fission products	Sr	2	0.146	0.146	0.146	0.146	0.165	0.165	0.265	0.265
	Y	3	0.078	0.117	0.078	0.117	0.089	0.134	0.141	0.212
	Zr	4	0.740	1.480	0.740	1.480	0.837	1.674	1.333	2.666
	Mo	4	0.264	0.528	0.263	0.526	0.298	0.596	0.478	0.950
	Cs	1	0.059	0.030	0.208	0.104	0.401	0.201	0.596	0.298
	Ba	2	0.238	0.238	0.237	0.237	0.269	0.269	0.428	0.428
	La	3	0.187	0.281	0.187	0.281	0.212	0.318	0.337	0.506
	Ce	4	0.367	0.734	0.367	0.734	0.416	0.832	0.662	1.324
	Pr	3	0.162	0.243	0.162	0.243	0.183	0.275	0.292	0.438
	Nd	3	0.611	0.917	0.610	0.917	0.691	2.037	1.101	1.652
	Sm	3	0.103	0.155	0.103	0.155	0.117	0.176	0.186	0.279
	Eu	3	0.013	0.020	0.013	0.020	0.015	0.023	0.023	0.035
	Gd	3	0.080	0.120	0.080	0.120	0.091	0.137	0.144	0.216
	Tb	3	0.002	0.003	0.002	0.003	0.002	0.003	0.003	0.005
	Dy	3	0.008	0.012	0.008	0.012	0.009	0.014	0.015	0.023
Total			32.722	64.169	32.823	64.148	32.870	63.793	32.604	62.169
O/M ratio			1.967		1.960		1.948		1.918	

Une and Oguma [20] report from studies on UO_2 doped with soluble fission product elements to simulate burn-ups up to 10 at.%, that the $\Delta\overline{G}(O_2)$ of UO_2 fuel increases linearly with burn-up at constant temperature. This is consistent with the earlier results of Woodley [19] obtained on $(U_{0.75}Pu_{0.25})O_2$ also doped with fission product elements to simulate burn-ups up to 10 at.%. In contradiction to these findings, the $\Delta\overline{G}(O_2)$ of the high burn-up fuel examined in this work did not increase linearly with the radial increase in the local burn-up. Although, a straight line can be drawn through the $\Delta\overline{G}(O_2)$ values measured at $r/r_0 = 0.1$, 0.5 and 0.8 when plotted as a function of the local burn-up, the value measured at $r/r_0 = 0.975$ does not continue the linear trend. The $\Delta\overline{G}(O_2)$ at the pellet rim (-292 kJ mol^{-1}), although higher than that in the body of the fuel, is substantially lower than it ought to be (-135 kJ mol^{-1}) if it were directly dependent on the local burn-up, that is, dependent on the fission product inventory. It is to be noted that Matzke [15] also found that in the rim region of the fuel with an average burn-up of 75 MWd/kgU the $\Delta\overline{G}(O_2)$ did not increase in accordance with the local burn-up. The lower then expected $\Delta\overline{G}(O_2)$ at the pellet rim is attributed primarily to an increase in the quantity of oxide second phases present in this region (see Table 5). In the rim region, owing to the low temperature of the fuel and the high concentration of the fission products present, it is likely that the solubility limit of a number of fission products will have been exceeded. The gettering effect of Zircaloy as indicated e.g., by Kleykamp [10,11] may also contribute to a small extent to the levelling of the oxygen potential increase near the pellet periphery (see below in this section).

An important result from the $\Delta\overline{G}(O_2)$ measurements on the high burn-up fuel with an average burn-up of 102 MWd/kgHM is that the $\Delta\overline{G}(O_2)$ is still increasing at this very high burn-up. Matzke [14] considered that the $\Delta\overline{G}(O_2)$ values he measured on a fuel with a burn-up of 75 MWd/kgHM represented an upper limit imposed by the buffering effect of the oxidation of fission product Mo. The $\Delta\overline{G}(O_2)$ results for the fuel an average burn-up of 102 MWd/kgHM, however, reveal this not to be the case. Since the $\Delta\overline{G}(O_2)$ of this fuel is actually higher than the free energy of formation of MoO_2, which at 500–1000 °C is about -410 to -390 kJ mol^{-1} (see e.g., Ref. [8]), it is clear that at high burn-up the $\Delta\overline{G}(O_2)$ of UO_2 fuel is not buffered by the oxidation of Mo. Very likely, with the exception of the rim values,

the $\Delta\overline{G}(O_2)$ values measured on the two fuels with burn-ups of 75 [14] and 102 MWd/kgHM are those that result directly from the liberation of oxygen by the fission process.

The O/U and O/M of the fuel at the radial positions where the oxygen potential was measured as determined from the UO_2 lattice parameter and the composition of the fuel, respectively, are compared in Table 7. It is evident that O/M ratio of the fuel is considerably lower than the O/U ratio of the fuel. As can be seen from Fig. 7(b) the O/U ratio varies little between the fuel centre and $r/r_0 = 0.96$, but then falls noticeably in the rim region. The decrease in the O/U in the vicinity of the fuel surface is mainly attributed to the steep increase in burn-up in this region (Fig. 1), that is, to the steep increase in the concentration of elements (actinides and fission products) that combine with oxygen. It is also evident from Fig. 7(b) that the formation of the high burn-up structure, which extends from the fuel surface to $r/r_0 = 0.66$ [26], is not associated with any significant change in the O/U ratio.

In Table 8 the O/M ratio of the fuel is compared with the stoichiometric O/M ratio at the radial positions where the $\Delta\overline{G}(O_2)$ measurements were performed. The difference between the two values of the O/M ratio corresponds to the local amount of active oxygen in the system. The O/M ratios given in Table 8 are plotted in Fig. 8. It can be seen from the figure that the amount of free (active) oxygen increases in the vicinity of the fuel periphery. This is mainly due to the decrease in the stoichiometric O/M ratio in this region, which is related to the increase in the local burn-up. The build-up of free oxygen at the pellet rim is unlikely to be the result of the radial transport of oxygen down the temperature gradient because during the last seven radiation cycles the fuel temperature was below 1000 °C. Moreover, the driving force for oxygen migration in LWR fuel is low in stoichiometric UO_2 because there is a dip in the heat of transport, Q, for the radial flux of material [39]. For the purpose of completion, the fuel O/M ratio and the stoichiometric O/M ratio calculated assuming that all the Mo measured by ICP-MS was present in the fuel in the metallic form are included in Fig. 8. Concerning the amount of free oxygen present in the fuel lattice this represents the extreme case.

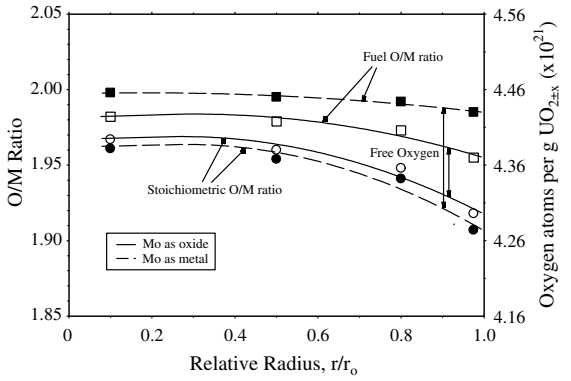

Fig. 8. Fuel and stoichiometric O/M ratios and the quantity of free oxygen as a function of radial position in the high burn-up fuel.

Also included in Table 8 are the O/M ratios at the end-of-life calculated assuming that the O/M ratio changes by 0.0013 per at.% burn-up as estimated by Kleykamp [10,11]. It can be seen from Table 8 that in agreement with Kleykamp's relationship the results of the oxygen balance calculation indicate that at the radial positions where the $\Delta\overline{G}(O_2)$ measurements were made the high burn-up fuel was hyperstoichiometric. The degree of hyperstoichiometry, Δ(O/M), is, however, about five times larger than predicted by Kleykamp's

Table 7
O/U and O/M ratios at the radial positions where the oxygen potential was measured as determined from the UO_2 lattice parameter and the composition of the fuel

Radial position (r/r_0)	O/U ratio	O/M ratio
0.10	1.995 ± 0.008	1.982
0.50	1.995 ± 0.008	1.979
0.80	1.990 ± 0.008	1.973
0.975	1.998 ± 0.008	1.955

Table 8
Comparison of the fuel O/M ratio with the stoichiometric O/M ratio for all actinides and oxide forming fission products at the radial positions where the oxygen potential measurements were made

Radial position (r/r_0)	Burn-up (MWd/kgHM)	O/M ratio		Δ(O/M)	O/M ratio after Kleykamp[a]
		Fuel[b]	Stoichiometric value		
0.10	88	1.982	1.967	0.015	2.012
0.50	88	1.979	1.960	0.019	2.012
0.80	100	1.973	1.948	0.025	2.014
0.975	162	1.955	1.918	0.037	2.022

[a] Assuming that the average shift in stoichiometry Δ(O/M) = 0.0013 per at.% burn-up [10,11].
[b] From the composition of the fuel.

relationship. The change would be expected to be somewhat larger in the present case, because about two-thirds of the burn-up accumulated in the high burn-up fuel was the result of Pu fission, which produces more noble fission products and less Sr, Y and Zr then U fission.

Kleykamp [10,11] concluded that in the case of high power fuel rods the excess oxygen released by fission is completely gettered by the Zircaloy cladding and consequently the stoichiometry of the fuel does not change significantly during irradiation. Since the high burn-up fuel investigated in this work was irradiated at low linear power (see Table 2) and hence at low temperature, the Zircaloy cladding would be expected to be less effective in controlling the build-up of oxygen in the fuel. This is supported by the post-irradiation examination results for the high burn-up rod which reveal that at the axial position from which the high burn-up fuel was cut the average thickness of the internal ZrO_2 layer was about 6 μm. The O/M ratio determined from the fuel composition neglects the gettering effect of the cladding, whereas the O/U ratio derived from the lattice parameter takes this into account. The O/M and O/U ratios obtained by these two different routes are compared in Table 7 where it is seen that fuel O/M ratio is markedly lower than the O/U ratio. About 9.9×10^{19} oxygen atoms from the fuel are needed to produce an internal oxide layer 6 μm on a 1 cm long section of cladding. The loss of this amount of oxygen would result in a decrease of the average O/M ratio of 0.007. For the calculation of the quantity of oxygen gettered by the cladding and the resulting change in the O/M ratio of the fuel the density of ZrO_2 was taken to be 5.6 g cm^3 and the fuel density at the end-of-life was used, which was 86.5% TD.

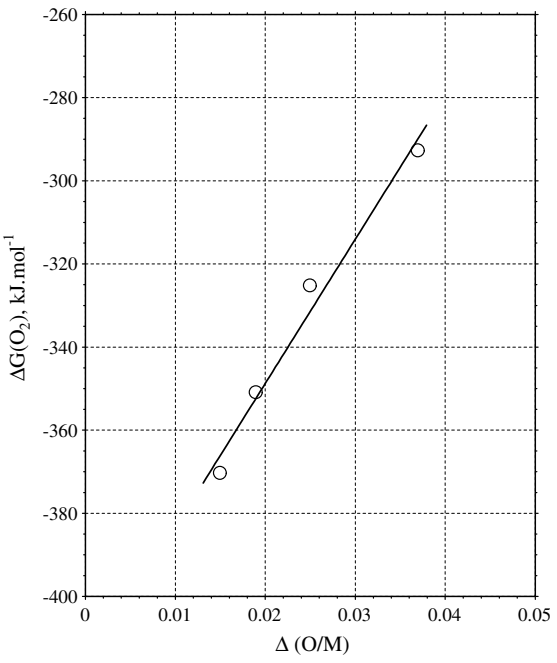

Fig. 9. Measured $\Delta G(O_2)$ at 750 °C as a function of Δ(O/M) representing the concentration of free oxygen derived from the difference between the local fuel O/M ratio and the local stoichiometric O/M ratio.

Comparison of the quantity of oxygen contained in the ZrO_2 layer on the inner surface of the cladding with the amount of free oxygen in the fuel cross-section reveals that less than one-quarter (22.6%) of the total free oxygen released by fission had been gettered by the Zircaloy cladding. The total amount of free oxygen in the fuel at end-of-life is taken to be the difference between the average O/M ratio of the fuel (1.973) and the average stoichiometric O/M ratio (1.949) obtained from the data in Table 6. This corresponds to 3.4×10^{20} oxygen atoms. As can be seen from Fig. 9, a linear relation exists between the local $\Delta\overline{G}(O_2)$ of the fuel measured at 750 °C and the local amount of free oxygen present as represented by the local difference between the fuel O/M ratio and the stoichiomteric O/M ratio. This is consistent with theory and implies that the fuel O/M ratio and stoichiometric O/M ratio have been correctly derived.

8. Summary and conclusions

From the results presented in this paper it can be concluded that the $\Delta\overline{G}(O_2)$ of UO_2 is still evolving at a high burn-up of 102 MWd/kgHM. The continuous increase in the $\Delta\overline{G}(O_2)$ is due to the fact that with increase in burn-up less of the free oxygen released by fission is bound by fission products in solid solution. Since the measured $\Delta\overline{G}(O_2)$ values were substantially higher than the free energy of formation of MoO_2 it is evident that the oxidation of fission product Mo does not buffer the $\Delta\overline{G}(O_2)$ of high burn-up fuel has concluded by Matzke [14].

The average O/U of the fuel decreased during irradiation from 2.005 to 1.991 ± 0.008. Thus, contrary to accepted theory, irradiation had not resulted in the oxidation of the uranium dioxide. Though the uranium dioxide appears not to have oxidised, the fuel as a whole was found to be slightly hyperstoichiometric. This is deduced from the fact that the fuel O/M ratio is much higher than the stoichiometric O/M ratio. The degree of hyperstoichiometry was roughly a factor of 2.5 higher at the rim than at the pellet centre.

Less than one-quarter (23%) of the free oxygen accumulated during the irradiation had been removed from the fuel to form the oxide layer on the inner surface of the Zircaloy cladding. This finding appears to be consistent with the fact that most of the burn-up in the rod was accumulated at low linear power (<20 kW m^{-1}).

The presence of the high burn-up structure in the outer region of the fuel was not associated with any noticeable change in the local $\Delta\overline{G}(O_2)$ or stoichiometry of the fuel.

Acknowledgements

The work presented in this paper is part of a long-standing high burn-up programme being performed by Framatome ANP GmbH and the Swiss Nuclear Plant Goesgen. The authors would like to thank Goesgen for their fruitful co-operation and their continuing support.

References

[1] M.A. Mansouri, D.R. Olander, J. Nucl. Mater. 254 (1998) 22.
[2] M.S. Seltzer, J.S. Perrin, A.H. Clauer, B.A. Wilcox, Review of out-of-pile and in-pile creep of ceramic nuclear fuels, Battelle Memorial Institute, Columbus, OH, USA, 1971, (USAEC Report BMI-1906).
[3] W. Miekely, F.W. Felix, J. Nucl. Mater. 42 (1972) 297.
[4] Hj. Matzke, Radiat. Eff. 53 (1980) 219.
[5] L.A. Goldsmith, J.A.M. Douglas, Measurements on thermal conductivity of uranium oxide at 670–1270 K, Harwell, England, 1971, (UKAEA Report TGR 2103(w)).
[6] I.C. Hobson, R. Taylor, J.B. Ainscough, J. Phys. D 7 (1974) 1003.
[7] P.G. Lucuta, Hj. Matzke, R.A. Verrall, J. Nucl. Mater. 223 (1995) 51.
[8] H. Kleykamp, J. Nucl. Mater. 131 (1985) 221.
[9] J.H. Davies, F.T. Ewart, J. Nucl. Mater. 41 (1971) 143.
[10] H. Kleykamp, in: IAEA Specialists' Meeting on Internal Fuel Rod Chemistry, IWGPFT/3, 1979, p. 15.
[11] H. Kleykamp, J. Nucl. Mater. 84 (1979) 109.
[12] M.G. Adamson, E.A. Aitken, S.K. Evans, J.H. Davies, in: Thermodynamics of Nuclear Materials, vol. 1 (IAEA-SM-190/54, Vienna), 1974, p. 59.
[13] K. Une, Y. Tominaga, S. Kashiba, J. Nucl. Sci. Technol. (Jpn.) 28 (1991) 409.
[14] Hj. Matzke, J. Nucl. Mater. 223 (1995) 1.
[15] Hj. Matzke, J. Nucl. Mater. 208 (1994) 18.
[16] C.T. Walker, Concerning the Microstructure Changes that Occur at the Surface of UO_2 Pellets on Irradiation to High burn-up, The European Commission, Institute for Transuranium Elements, Germany, 1991 (Report KO291141).
[17] T.L. Marken, R.J. Bones, UKAEA Harwell, Report AERE-R 4178, 1962.
[18] K. Une, Y. Tominaga, S. Kashibe, J. Nucl. Sci. Technol. (Jpn.) 28 (1991) 409.
[19] R.E. Woodley, J. Nucl. Mater. 74 (1978) 290.
[20] K. Une, M. Oguma, J. Nucl. Sci. Technol. (Jpn.) 20 (1983) 844.
[21] T. Lindemer, J. Brynestad, J. Am. Ceram. Soc. 69 (1986) 867.
[22] N.A. Javed, J. Nucl. Mater. 43 (1972) 219.
[23] U. Benedict, M. Coquerelle, J. de Bueger, C. Defour, J. Nucl. Mater. 45 (1972/73) 217.
[24] J. Spino, D. Papaioannou, J. Nucl. Mater. 281 (2000) 146.
[25] K. Lassmann, J. Nucl. Mater. 150 (1987) 10.
[26] R. Manzel, C.T. Walker, J. Nucl. Mater. 301 (2002) 170.
[27] K. Lassmann, C. O'Carrell, J. van der Laar, C.T. Walker, J. Nucl. Mater. 208 (1994) 223.
[28] C. Walker, J. Anal. At. Spectrom. 14 (1999) 447.
[29] J. Spino, Safety of Nuclear Fuels: High Burn-up Performance, The European Commission, Institute for Transuranium Elements, Germany, 2001, p. 54, (Report Eur 20252 EN).
[30] M.J. Bell, ORIGEN – The ORNL isotope Generation and Depletion code, Oak Ridge National Laboratory, 1973 (Report ORNL-4623).
[31] B.D. Cullity, Elements of X-ray Diffraction, Addision-Wesley, Reading, MA, 1967, p. 352.
[32] D. Staicu, T. Wiss, C. Ronchi, in: Proceedings of the ANS Meeting on LWR Fuel Performance, Orlando, Fl, USA, 19–22 September 2004, paper 1087.
[33] V.V. Rondinella, Hj. Matzke, J. Cobos, T. Wiss, Mater. Res. Soc. Symp. Proc. 556 (1999) 447.
[34] F. Grønvold, J. Inorg. Nucl. Chem. 1 (1955) 357.
[35] D. Vollath, H. Wedemeyer, in: Uranium Oxide, 8th Ed., in: R. Keim (Ed.), Gmelin Handbook of Inorganic Chemistry, Supplimentary vol. C4, Springer, Berlin, 1984, p. 112.
[36] H. Kleykamp, J. Nucl. Mater. 206 (1993) 82.
[37] C.T. Walker, C. Bagger, M. Mogensen, J. Nucl. Mater. 240 (1996) 32.
[38] T.B. Lindemer, Calphad 10 (1986) 129.
[39] J. Janek, H. Timm, J. Nucl. Mater. 255 (1998) 116.